ACS APPLIED MATERIALS & INTERFACES

Letter

www.acsami.org

Brookite TiO_2 Thin Film Epitaxially Grown on (110) YSZ Substrate by Atomic Layer Deposition

Dai-Hong Kim, Won-Sik Kim, Sungtae Kim, and Seong-Hyeon Hong*

Department of Materials Science and Engineering and Research Institute of Advanced Materials (RIAM), Seoul National University, Seoul 151-744, Korea

Supporting Information

ABSTRACT: Epitaxial brookite TiO_2 (B-TiO_2) film was deposited on (110) yttria-stabilized zirconia (YSZ) substrate using plasma-enhanced atomic layer deposition, and its structural, optical, and gas sensing properties were investigated. As-deposited TiO_2 film was a pure brookite and (120) oriented. The determined in-plane orientation relationships were $[2\bar{1}0]_{B-TiO_2}//[\bar{1}10]_{YSZ}$ and $[001]_{B-TiO_2}//[001]_{YSZ}$. The B-$TiO_2$ film showed ~70% transmittance and the optical band gap energy was 3.29 eV. The B-TiO_2 film-based gas sensor responded to H_2 gas even at room temperature and the highest magnitude of the gas response was determined to be ~150 toward 1000 ppm of H_2/air at 150 °C. In addition, B-TiO_2 sensor showed a high selectivity for H_2 against CO, EtOH, and NH_3.

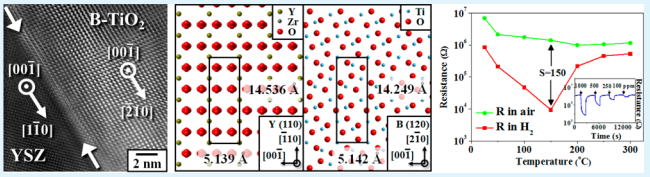

KEYWORDS: *TiO_2 film, brookite, atomic layer deposition, gas sensor, optical properties*

Titanium dioxide (TiO_2) is a well-known multifunctional material for a wide range of technological applications such as photocatalysis, photovoltaics, transparent conducting oxide (TCO), gas sensor, and lithium-ion battery (LIB).[1−7] In nature, TiO_2 exhibits three polymorphs: anatase (A-TiO_2, tetragonal), brookite (B-TiO_2, orthorhombic), and rutile (R-TiO_2, tetragonal).[8] Rutile is the thermodynamically stable form of TiO_2, whereas anatase and brookite are metastable and transform to the rutile phase upon heating.[9] Each crystalline phase has different optical, electrical, and photochemical properties, and the performance of TiO_2 strongly depends on the crystal structure, morphology, and size of the particles.[10,11] Anatase and rutile phases have been extensively studied and widely used in the form of powders and thin films. On the contrary, pure brookite phase is difficult to prepare in either form and there are a few reports on its electrochemical, photocatalytic, photovoltaic, and gas sensing properties.[5,12−16] B-TiO_2 showed higher photocatalytic activity, better photo-induced hydrophilicity, and higher volumetric energy density than the other phases, which suggest the potential applications as photocatalyst and anode for LIB.[5,13,15]

B-TiO_2 thin films have been prepared by various methods including pulse laser deposition (PLD),[17] dip-coating,[18−20] spin-coating,[15,21,22] metal organic chemical vapor deposition (MOCVD),[23] plasma-enhanced chemical vapor deposition (PECVD),[24] electron beam evaporation,[25] and matrix-assisted pulse laser evaporation (MAPLE).[16] However, most reported B-TiO_2 films contain the anatase or rutile phase as a secondary phase. In particular, epitaxial brookite TiO_2 film has not been reported yet, although epitaxial anatase and rutile TiO_2 films have been successfully fabricated on the singl-crystal substrates.[25−27] Among the various substrates, yttria-stabilized zirconia (YSZ) is suitable for epitaxial brookite considering the lattice mismatch,[25] but anatase or mixed (anatase and brookite) TiO_2 has been epitaxially grown on (100) YSZ.[25,27] In our previous work, epitaxial SnO_2 films were successfully grown on sapphire, TiO_2, and YSZ substrates by plasma enhanced atomic layer deposition (PEALD).[28−30] To the best of our knowledge, PEALD has not been applied for depositing an epitaxial brookite TiO_2 film.

In this work, B-TiO_2 film was epitaxially grown on a (110) YSZ substrate by PEALD and its in-plane orientation relationships with the substrate were determined using X-ray pole figure and high resolution transmission electron microscopy (HRTEM). The optical and gas sensing properties of obtained B-TiO_2 films were investigated, particularly focusing on the low temperature detection of H_2 gas because there is a tremendous demand for H_2 thin film gas sensors with high sensitivity, selectivity, and fast response, which can operate at room temperature and be integrated into the semiconductor devices such as portable electric noses.[31,32]

TiO_2 thin films were deposited on (110) YSZ substrate by PEALD. Titanium Isopropoxide (TTIP) ($Ti(OCH(CH_3)_2)_4$) was used as a Ti precursor, which was evaporated at room temperature and transported to the deposition chamber by 10 sccm Ar (99.99%). The 50 sccm O_2 (99.99%) and Ar (99.99%) were used as plasma and purge gases, respectively. The time sequence for the source pulse, first purge, O_2 pulse, O_2 plasma pulse, and second purge was 1, 12, 2, 10, and 12 s, respectively. The deposition was conducted with an rf power of 100 W at 220 mTorr for 1000 cycles, and the substrate temperature was maintained at 300 °C. The structural characteristics and the

Received: March 19, 2014
Accepted: July 9, 2014
Published: July 9, 2014

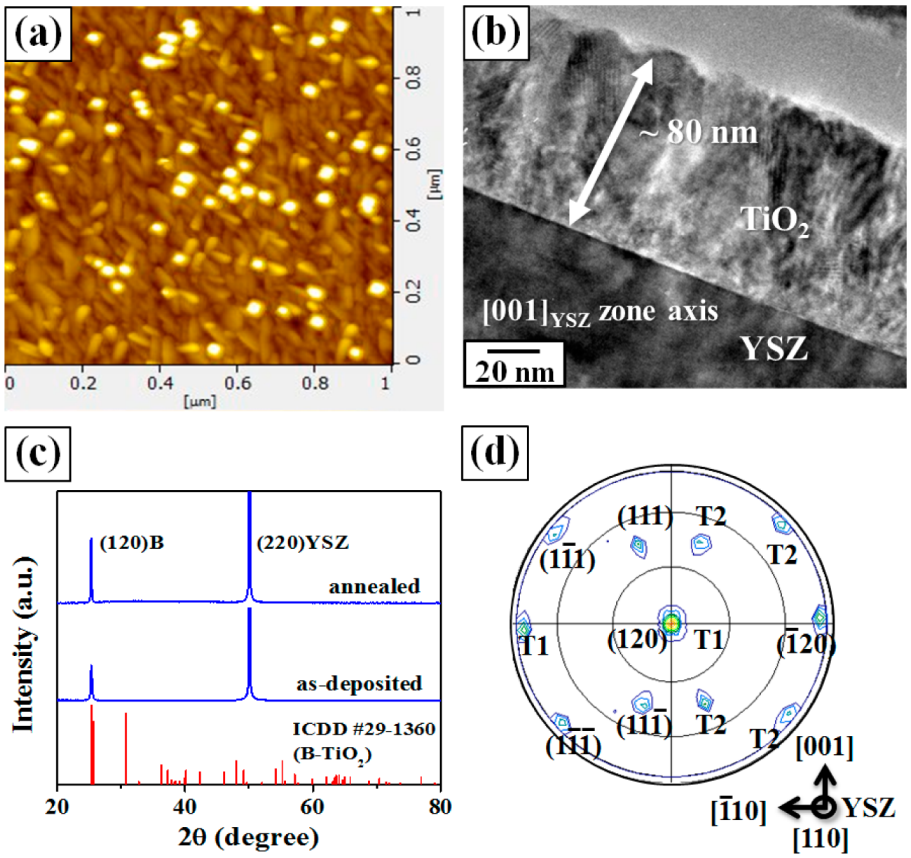

Figure 1. (a) Surface morphology observed by AFM and (b) cross-sectional TEM image of as-deposited TiO_2 film grown on (110) YSZ. (c) XRD patterns of as-deposited and annealed (at 700 °C for 1 h) TiO_2 films grown on (110) YSZ. The reference is the standard diffraction pattern of brookite TiO_2 (ICDD #29−1360). (d) {120} pole figure of as-deposited TiO_2 film grown on (110) YSZ.

optical and H_2 gas sensing properties of as-deposited films were examined. (for more experimental details, see the Supporting Information).

The surface morphology of as-deposited film observed by AFM is shown in Figure 1a. The surface was relatively rough, exhibiting an elongated granular morphology. The root-mean-square (RMS) value of the surface roughness was 4 nm (scan area 1 μm × 1 μm). The surface roughness was much improved when the substrate temperature was reduced to 100 °C (see Figure S1 in Supporting Information), but the crystallinity of the film decreased and thus, the substrate temperature was fixed to be 300 °C. The cross-sectional TEM image showed that the film thickness was ~80 nm (Figure 1b), which was also confirmed by X-ray reflectivity (XRR). The film density determined by XRR was ~3.95 g/cm^3, which was ~96% of the theoretical density for brookite TiO_2 (4.13 g/cm^3).[33] The chemical states of Ti and O in as-deposited film were determined by XPS (see Figure S2 in the Supporting Information). The film exhibited a Ti 2p doublet with a Ti $2p_{3/2}$ at 458.5 eV and a single peak of O 1s at 530.05 eV, which match well with those for stoichiometric TiO_2.[34] The XRD patterns of as-deposited film at 300 °C and annealed film are shown in Figure 1c. The deposited film was crystalline and only one peak was observed except the peak for YSZ substrate. The diffraction peak of film was indexed as (120) based on the orthorhombic brookite (B-TiO_2, ICDD #29−1360). Thus, highly oriented (120) B-TiO_2 was grown on the (110) YSZ substrate. The substrate temperature affected the structure of the TiO_2 film on YSZ. When the substrate temperature increased to 500 °C, B-TiO_2 was changed to the mixed phases of B-TiO_2 and R-TiO_2 (see Figure S3 in the Supporting Information). In order to investigate the thermal stability, as-deposited film (300 °C) was annealed at 700 °C for 1 h, but no phase change was observed. Thus, the obtained B-TiO_2 film was thermally stable, which is believed to be due to the constraint from the substrate (epitaxial relationship). It is known that a brookite phase is transformed into an anatase or rutile phase at over 500 °C.[35,36] In addition, Raman spectroscopy was employed to further confirm the brookite phase,[5,37] but the signals were very weak and overlapped with those of the YSZ substrate and thus, the phase identification was not possible. The in-plane orientation relationship between the film and substrate was investigated using an X-ray pole figure. The {120} pole figure of B-TiO_2 film is shown in Figure 1d, where the substrate orientation is indicated next to the pole figure. The reflections from {120} family planes ((120) and ($\bar{1}$20)) appeared with additional contributions from 180° rotation marked as T1 in the figure. The appearance of 180° rotated reflections is due to the 2-fold symmetry of (110) YSZ and the nonsymmetry of (120) B-TiO_2, implying two variants in the film. The 180° rotated contribution has been frequently observed in epitaxially grown TiO_2 films.[38] In the pole figure, the reflections from the {111} family of planes were detected because the diffraction angles of (111) and (120) were very close (25.689° vs 25.339°). The in-plane relationship was determined to be $[2\bar{1}0]_{B-TiO_2}//[\bar{1}10]_{YSZ}$ and $[001]_{B-TiO_2}//[001]_{YSZ}$.

To confirm the epitaxial growth, we further examined the B-TiO_2 film by high-resolution transmission electron microscopy (HRTEM). Images a and b in Figure 2 show the cross-sectional

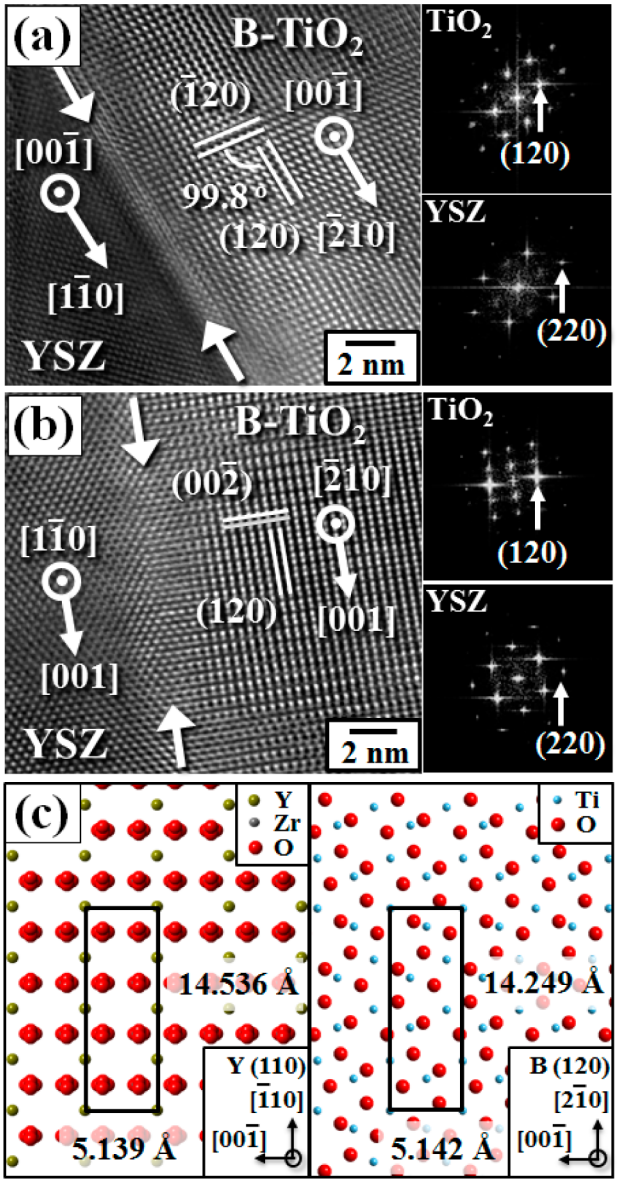

Figure 2. HRTEM images and FFT patterns for B-TiO_2 film and YSZ viewed along (a) [00$\bar{1}$] and (b) [1$\bar{1}$0] directions of YSZ. (c) Schematic diagrams of in-plane atomic configurations for (120) B-TiO_2 film and (110) YSZ substrate.

HRTEM images of TiO_2 film along with fast Fourier transformation (FFT) patterns from the film and substrate. The interfaces between the film and substrate were well-defined and atomistically sharp. The HRTEM image, viewed along the [00$\bar{1}$] direction of YSZ (Figure 2a), exhibited a (120) lattice fringe parallel to the interface and a ($\bar{1}$20) lattice fringe with an angle of 99.8° to the interface. The FFT patterns confirmed that the (120) B-TiO_2 film grew epitaxially on the (110) YSZ substrate with the orientation relationship of $[2\bar{1}0]_{B-TiO_2}$//$[\bar{1}10]_{YSZ}$ and $[001]_{B-TiO_2}$//$[001]_{YSZ}$. In the some parts of the film, 180° rotated (120) B-TiO_2 film was observed with (120) B-TiO_2, which was consistent with the X-ray pole figure (see Figure S4 in the Supporting Information). The HRTEM image, viewed along the [1$\bar{1}$0] direction of YSZ (Figure 2b), exhibited (120) and (00$\bar{2}$) lattice fringes parallel and perpendicular to the interface, respectively, and the obtained in-plane orientation relationship between film and substrate was also confirmed. Based on the determined epitaxial relationship, the in-plane atomic configurations of (120) B-TiO_2 and (110) YSZ are schematically shown in Figure 2c. The estimated lattice mismatch in each direction was −1.91 and 0.06%, respectively, based on the reported lattice parameters of $a(TiO_2)$ = 5.455, $b(TiO_2)$ = 9.181, $c(TiO_2)$ =5.142, (B-TiO_2, ICDD #29−1360), and a(YSZ) = 5.139 Å (YSZ, ICDD #30−1468). The lattice mismatches in both directions are quite small, and thus (120) B-TiO_2 can be heteroepitaxially grown on (110) YSZ substrate.

Figure 3 shows the optical transmittance spectra of as-deposited B-TiO_2 film on (110) YSZ and bare (110) YSZ

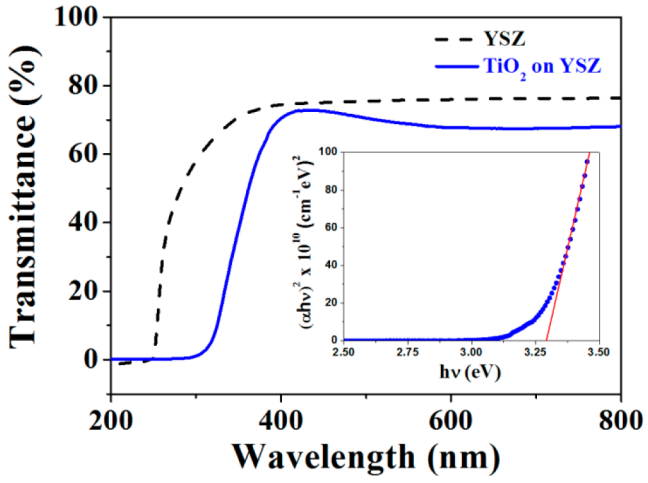

Figure 3. Optical transmittance spectra of B-TiO_2 film and bare YSZ substrate. The inset shows a plot of $(\alpha E)^2$ vs E for B-TiO_2 film.

substrate as a function of wavelength in the range of 200−800 nm. The average transmittance in the visible region (400−700 nm) was about 70%, which was slightly lower than that of the bare YSZ substrate. The film showed a strong absorption in the UV region (250−400 nm). From the plots of $(\alpha E)^2$ vs photon energy (E), the optical band gap energy (E_g) was determined by extrapolating the straight line portion of the plot. The determined E_g was ~3.29 eV, which was close to the reported value for the B-TiO_2 nanorod and still higher than that for rutile (3.0 eV) and anatase (3.2 eV).[10,39]

Figure 4a shows a typical response transient of the B-TiO_2 film sensor toward H_2 gas balanced with air measured at 150 °C. The H_2 concentration was varied from 1000 to 100 ppm in discrete steps. The sensor exhibited a decrease in resistance upon injecting the H_2 gas and recovered to the original level after removing the H_2 gas. The sensing signal was stable and reproducible. The magnitude of the gas response (S) was defined as the ratio (R_{air}/R_{gas}) of the resistance in air (R_{air}) to that in a sample gas (R_{gas}). It was determined to be ~150 at 1000 ppm of H_2/air and decreased with decreasing H_2 concentration. The determined magnitude of gas response (S) toward 1000 ppm of H_2/air is shown in Figure 4b as a function of sensing temperature. For comparison, the gas response of (200) R-TiO_2 film coated on a-cut (110) sapphire in the same deposition conditions was included (see Figure S5 in the Supporting Information). The B-TiO_2 film sensor detected the H_2 gas even at room temperature and the highest

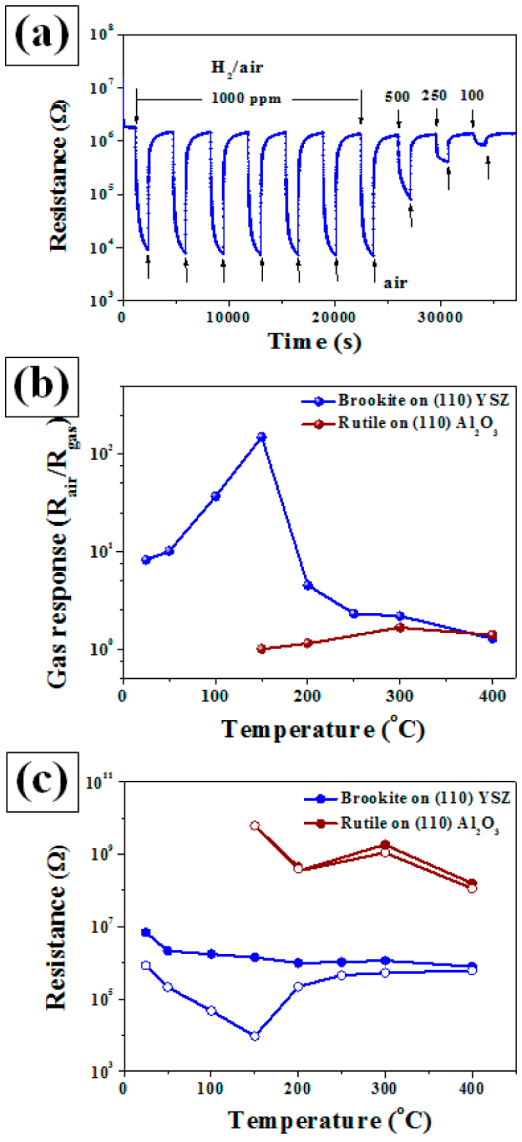

Figure 4. (a) Typical response transient of the B-TiO_2 film toward H_2 gas/air (1000−100 ppm) measured at 150 °C. (b) Magnitude of gas response toward 1000 ppm of H_2/air in the films grown on (110) YSZ and (110) Al_2O_3 substrates as a function of sensing temperature. (c) Electrical resistances of the films grown on (110) YSZ and (110) Al_2O_3 substrates in air and 1000 ppm of H_2/air as a function of operating temperature. (closed circles: resistance in air (R_{air}), open circles: resistance in 1000 ppm of H_2/air (R_{gas})).

H_2 gas response was obtained at 150 °C, which is a characteristic behavior of semiconductor-type gas sensors.[40] The magnitude of gas response obtained at room temperature was lower than the best value reported in the TiO_2 nantube-array sensor,[32] but the present B-TiO_2 film sensor was one of a few TiO_2-based gas sensors, which can detect the H_2 gas in air balance. As mentioned earlier, the brookite phase was stable up to 700 °C and thus, the B-TiO_2 film sensor is expected to be more thermally stable than the other nanostructure-based TiO_2 sensors. The optimum working temperature of 150 °C in B-TiO_2 film sensor was much lower than the previously reported rutile TiO_2 film sensors and comparable to that of the A-TiO_2 nanotube sensor.[31,41,42] On the other hand, the (200) R-TiO_2 film sensor showed the H_2 gas response above 150 °C and the magnitude of gas response was comparatively lower. At 150 °C, the magnitude of gas response was 2 orders of magnitude lower than that of B-TiO_2 sensor.

To further investigate the low temperature H_2 detection of B-TiO_2 sensor, the temperature dependence of the electrical resistance is shown in Figure 4c. The electrical resistance of R-TiO_2 sensor was beyond the detection limit of the equipment (>1 × 10^{10} Ω) and thus, the sensor measurement was possible above 150 °C and the resistance change with H_2 exposure was small resulting in the lower magnitude of gas response. However, in B-TiO_2 sensor, both R_{air} and R_{gas} were within the detection limit even at room temperature and the sensor stably responded to H_2 gas at low temperatures. R_{air} was relatively constant with temperature whereas R_{gas} decreased with increasing temperature from room temperature to 150 °C and then increased with a further increase of temperature, which resulted in the highest gas response at 150 °C. Consequently, B-TiO_2 film had the lower resistance and higher resistance change with H_2 exposure or adsorption/desorption of oxygen species than R-TiO_2 film, which lead to the superior H_2 gas detection at low temperature. We have also deposited the TiO_2 films on (100) and (111) YSZ and examined the H_2 gas sensing properties. The film deposited (100) YSZ was oriented anatase-brookite mixture consistent with previous report[25] whereas the film deposited on (111) YSZ was nonoriented anatase-brookite mixture (see Figure S6 in the Supporting Information). The magnitude of H_2 gas response in TiO_2 film deposited on (100) YSZ was comparable to that of B-TiO_2 and the film deposited on (111) YSZ exhibited the very low H_2 gas response (see Figure S7 in the Supporting Information). At this stage, it is difficult to relate the H_2 gas sensing performance to the crystallographic orientation in B-TiO_2 film because of mixed phases. The sensing properties of B-TiO_2 film sensor toward CO, ethanol (EtOH), and NH_3 gases were also investigated (see Figure S8 in the Supporting Information). The magnitude of gas response for CO, EtOH, and NH_3 was an order of magnitude lower than that for H_2 gas. Thus, B-TiO_2 film sensor showed a high selectivity for H_2 against CO, EtOH, and NH_3, particularly at low temperature. The high selectivity for H_2 against other gases in TiO_2−based gas sensors has been attributed to the catalytic effect of Pt electrode and hydrogen chemisorption which acts as an electron donor.[31,43]

In summary, B-TiO_2 film was successfully deposited on (110) YSZ substrate at 300 °C by PEALD. TiO_2 film was epitaxially grown on YSZ substrate, and the heteroepitaxial relationships were determined by XRD, pole figure, and HRTEM. As-deposited film was thermally stable, and the brookite phase was maintained up to 700 °C. The average transmittance of B-TiO_2 film was about 70% in the visible range, and the optical band gap energy was estimated to be 3.29 eV. The B-TiO_2 film sensor stably responded to H_2 gas in air at a relatively low temperature. The maximum gas response toward H_2 gas was observed at 150 °C and B-TiO_2 film sensor exhibited the high selectivity for H_2 against CO, EtOH, and NH_3.

■ ASSOCIATED CONTENT

Ⓢ Supporting Information

Experimental details and Figure S1−S8. This material is available free of charge via the Internet at http://pubs.acs.org

AUTHOR INFORMATION

Corresponding Author

*E-mail: shhong@snu.ac.kr. Tel: +82-2-880-6273. Fax: +82-2-884-1413.

Notes

The authors declare no competing financial interest.

ACKNOWLEDGMENTS

This research was supported by the National Research Foundation of Korea (NRF) grant funded by the Korea government (MSIP) (NRF- 2012R1A2A4A01008226).

REFERENCES

(1) Linsebigler, A. L.; Lu, G., Jr.; Yates, J. T. Photocatalysis on TiO_2 Surfaces: Principles, Mechanisms, and Selected Results. *Chem. Rev.* **1995**, *95*, 735−758.

(2) Ito, S.; Zakeeruddin, S.; Humphry-Baker, M. R.; Liska, P.; Charvet, R.; Comte, P.; Nazeeruddin, M. K.; Péchy, P.; Takata, M.; Miura, H.; Uchida, S.; Grätzel, M. High-Efficiency Organic-Dye-Sensitized Solar Cells Controlled by Nanocrystalline-TiO_2 Electrode Thickness. *Adv. Mater.* **2006**, *18*, 1202−1205.

(3) Gillispie, M. A.; van Hest, M. F.A.M.; Dabney, M. S.; Perkins, J. D.; Ginley, D. S. Sputtered Nb- and Ta-doped TiO_2 Transparent Conducting Oxide Films on Glass. *J. Mater. Res.* **2007**, *22*, 2832−2837.

(4) Shimizu, Y.; Kuwano, N.; Hyodo, T.; Egashira, M. High H_2 Sensing Performance of Anodically Oxidized TiO_2 Film Contacted with Pd. *Sens. Actuators, B* **2002**, *83*, 195−201.

(5) Dambournet, D.; Belharouak, I.; Amine, K. Tailored Preparation Methods of TiO_2 Anatase, Rutile, Brookite: Mechanism of Formation and Electrochemical Properties. *Chem. Mater.* **2010**, *22*, 1173−1179.

(6) Gao, P.; Bao, D.; Wang, Y.; Chen, P.; Wang, L.; Yang, S.; Chen, G.; Li, G.; Sun, Y. Qin, Wei. Epitaxial Growth Route to Crystalline TiO_2 Nanobelts with Optimizable Electrochemical Perfomance. *ACS Appl. Mater. Interface* **2013**, *5*, 368−373.

(7) Xin, X.; Zhou, X.; Wu, J.; Yao, X.; Liu, Z. Scalable Synthesis of TiO_2/Graphene Nanostructured Composite with High-Rate Perfomance for Lithium Ion Batteries. *ACS Nano* **2012**, *6*, 11035−11043.

(8) Zhang, Y.-F.; Lin, W.; Li, Y.; Ding, K.-N.; Li, J.-Q. A Theoretical Study on the Electronic Structures of TiO_2: Effect of Hartree-Fock Exchange. *J. Phys. Chem. B* **2005**, *109*, 19270−19277.

(9) Hu, Yi; Tsai, H.-L.; Huang, C.-L. Effect of Brookite Phase on the Anatase−Rutile Transition in Titania Nanoparticles. *J. Eur. Ceram. Soc.* **2003**, *23*, 691−696.

(10) Li, J.-G.; Ishigaki, T.; Sun, X. Anatase, Brookite, and Rutile Nanocrystals via Redox Reactions under Mild Hydrothermal Conditions: Phase-Selective Synthesis and Physicochemical Properties. *J. Phys. Chem. C* **2007**, *111*, 4969−4976.

(11) Hu, W.; Li, L.; Li, G.; Tang, C.; Sun, L. High-Quality Brookite TiO_2 Flowers: Synthesis, Characterization, Dielectric Performance. *Cryst. Growth Des.* **2009**, *9*, 3676−3682.

(12) Reddy, M. A.; Pralong, V.; Varadaraju, U. V.; Raveau, B. Crystallite Size Constraints on Lithium Insertion into Brookite TiO_2. *Electrochem. Solid-State Lett.* **2008**, *11* (8), A132−A134.

(13) Ohtani, B.; Handa, J.; Nishimoto, S.; Kagiya, T. Highly Active Semiconductor Photocatalyst; Extra-fine Crystallite of Brookite TiO_2 for Redox Reaction in Aqueous Propan-2-ol and /or Silver Sulfate Solution. *Chem. Phys. Lett.* **1985**, *120*, 292−294.

(14) Koelsch, M.; Cassaignon; Guillemoles, J. F.; Jolivet, J. P. Comparison of Optical and Electrochemical Properties of Anatase and Brookite TiO_2 Synthesized by Sol-Gel Method. *Thin Solid Films* **2002**, *403*−*404*, 312−319.

(15) Shibata, T.; Irie, H.; Ohmori, M.; Nakajima, A.; Watanabea, T.; Hashimoto, K. Comparison of Photochemical Properties of Brookite and Anatase TiO_2 Films. *Phys. Chem. Chem. Phys.* **2004**, *6*, 1359−1362.

(16) Caricato, A. P.; Buonsanti, R.; Catalano, M.; Cesaria, M.; Cozzoli, P. D.; Luches, A.; Manera, M. G.; Martino, M.; Taurino, A.; Rella, R. Films of Brookite TiO_2 Nanorods/ Nanoparticles Deposited by Matrix-Assisted Pulsed Laser Evaporation as NO_2 Gas-Sensing Layers. *Appl. Phys. A: Mater. Sci. Process.* **2011**, *104*, 963−968.

(17) Moret, M. P.; Zallen, R.; Vijay, D. P.; Desu, S. B. Brookite-Rich Titania Films made by Pulsed Laser Deposition. *Thin Solid Films* **2000**, *366*, 8−10.

(18) Djaoueda, Y.; Brüning, R.; Bersanic, D.; Lotticic, P. P.; Badilescu, S. Sol−Gel Nanocrystalline Brookite-Rich Titania Films. *Mater. Lett.* **2004**, *58*, 2618−2622.

(19) Addamo, M.; Bellardita, M.; Paola, A. D.; Palmisano, L. Preparation and Photoactivity of Nanostructured Anatase, Rutile and Brookite TiO_2 Thin Films. *Chem. Commun.* **2006**, 4943−4945.

(20) Paola, A. D.; Addamo, M.; Bellardita, M.; Cazzanelli, E.; Palmisano, L. Preparation of Photocatalytic Brookite Thin Films. *Thin Solid Films* **2007**, *515*, 3527−3529.

(21) Kuznetsova, I. N.; Blaskov, V.; Stambolova, I.; Znaidi, L.; Kanaev, A. TiO_2 Pure Phase Brookite with Preferred Orientation, Synthesized as a Spin-Coated Film. *Mater. Lett.* **2005**, *59*, 3820−3823.

(22) Moonoosawmy, K. R.; Katzke, H.; Es-Souni, M.; Dietze, M.; Es-Souni, M. Mesoporous and Macroporous Brookite Thin Films Having a Large Thermal Stability Range. *Langmuir* **2012**, *28*, 6706−6713.

(23) Leistner, T.; Lehmbacher, K.; Härter, P.; Schmidt, C.; Bauer, A. J.; Frey, L.; Ryssel, H. MOCVD of Titanium Dioxide on the Basis of New Precursors. *J. Non-Cryst. Solids* **2002**, *303*, 64−68.

(24) Srivatsa, K. M. K.; Bera, M.; Basu, A. Pure Brookite Titania Crystals with Large Surface Area Deposited by Plasma Enhanced Chemical Vapour Deposition Technique. *Thin Solid Films* **2008**, *516*, 7443−7446.

(25) Lotnyk, A.; Senz, S.; Hesse, D. Epitaxial Growth of TiO_2 Thin Films on $SrTiO_3$, $LaAlO_3$ and Yttria-Stabilized Zirconia Substrates by Electron Beam Evaporation. *Thin Solid Films* **2007**, *515*, 3439−3447.

(26) Yamamoto, S.; Sumita, T.; Sugiharuto; Miyashita, A.; Naramoto, H. Preparation of Epitaxial TiO_2 Films by Pulsed Laser Deposition Technique. *Thin Solid Films* **2001**, *401*, 88−93.

(27) Yamamoto, S.; Sumita, T.; Yamaki, T.; Miyashita, A.; Naramoto, H. Characterization of Epitaxial TiO_2 Films Prepared by Pulsed Laser Deposition. *J. Cryst. Growth* **2002**, *237*−*239*, 569−573.

(28) Kim, D. H.; Kim, W.-S.; Lee, S. B.; Hong, S.-H. Gas Sensing Properties in Epitaxial SnO_2 Films Grown on TiO_2 Single Crystals with Various Orientations. *Sens. Actuators, B* **2010**, *147*, 653−659.

(29) Kim, D. H.; Kwon, J.-H.; Kim, M.; Hong, S.-H. Structural Characteristics of Epitaxial SnO_2 Films Deposited on a- and m-cut Sapphire by ALD. *J. Cryst. Growth* **2011**, *322*, 33−37.

(30) Kim, S.; Kim, D.-H.; Hong, S.-H. Epitaxial Growth of Orthorhombic SnO_2 Films on Various YSZ Substrates by Plasma Enhanced Atomic Layer Deposition. *J. Cryst. Growth* **2012**, *348*, 15−19.

(31) Lee, J.; Kim, D. H.; Hong, S.-H.; Jho, J. Y. A Hydrogen Gas Sensor Employing Vertically Aligned TiO_2 Nanotube Arrays Prepared by Template-Assisted Method. *Sens. Actuators, B* **2011**, *160*, 1494−1498.

(32) Chen, K.; Xie, K.; Feng, X.; Wang, S.; Hu, R.; Gu, H.; Li, Y. An Excellent Room-temperature Hydrogen Sensor Based on Titania Nanotube-Arrays. *Int. J. Hydrogen Energy* **2012**, *37*, 13602−13609.

(33) Kim, H. G.; Kim, K. T. Densification Behavior of Nanocrystalline Titania Powder Compact under High Temperature. *Acta Mater.* **1999**, *47*, 3561−3570.

(34) Moulder, J. F.; Stickle, W. F.; Sobol, P. E.; Bomben, K. D. *Handbook of X-ray Photoelectron Spectroscopy: A Reference Book of Standard Spectra for Identification and Interpretation of XPS Data*; Physical Electronics: Eden Prarie, MN, 1995.

(35) Zhang, H.; Banfield, J. F. Understanding Polymorphic Phase Transformation Behavior during Growth of Nanocrystalline Aggregates: Insights from TiO_2. *J. Phys. Chem. B* **2000**, *104*, 3481−3487.

(36) Li, J.-G.; Ishigaki, T. Brookite→Rutile Phase Transformation of TiO_2 Studied with Monodispersed Particles. *Acta Mater.* **2004**, *52*, 5143−5150.

(37) Tompsett, G. A.; Bowmaker, G. A.; Cooney, R. P.; Metson, J. B.; Rodgers, K. A.; Seakins, J. M. The Raman Spectrum of Brookite, TiO_2 (Pbca, Z = 8). *J. Raman Spectrosc.* **1995**, *26*, 57−62.

(38) Gao, Y.; Merkle, K. L.; Chang, H. L.; Zhang, T. J.; Lam, D. J. Study of Defects and Interfaces on the Atomic Scale in Epitaxial TiO_2 Thin Films on Sapphire. *Philos. Mag. A* **1992**, *65* (5), 1103−1125.
(39) Kandiel, T. A.; Feldhoff, A.; Robben, L.; Dillert, R.; Bahnemann, D. W. Tailored Titanium Dioxide Nanomaterials: Anatase Nanoparticles and Brookite Nanorods as Highly Active Photocatalysts. *Chem. Mater.* **2010**, *22*, 2050−2060.
(40) Yamazoe, N.; Sakai, G.; Shimanoe, K. Oxide Semiconductor Gas Sensors. *Catal. Surv. Asia* **2003**, *7*, 63−75.
(41) Epifani, M.; Helwig, A.; Arbiol, J.; Díaz, R.; Francioso; Siciliano, L. P.; Mueller, G.; Morante, J. R. TiO_2 Thin Films from Titanium Butoxide: Synthesis, Pt Addition, Structural Stability, Microelectronic Processing and Gas-Sensing Properties. *Sens. Actuators, B* **2008**, *130*, 599−608.
(42) Moon, W.-T.; Lee, K.-S.; Jun, Y.-K.; Kim, H.-S.; Hong, S.-H. Orientation Dependence of Gas Sensing Properties of TiO_2 Films. *Sens. Actuators, B* **2006**, *115*, 123−127.
(43) Varghese, O. K.; Gong, D.; Paulose, M.; Ong, K. G.; Grimes, C. A. Hydrogen Sensing Using Titania Nanotubes. *Sens. Actuator, B* **2003**, *93*, 338−344.